

Impact of polarization mode dispersion on entangled photon distribution

VADIM RODIMIN^{1,*}, KONSTANTIN KRAVTSOV¹, RUI MING CHUA^{1,2}, GIANLUCA DE SANTIS¹, ALEKSEI PONASENKO¹, YURY KUROCHKIN¹, ALEXANDER LING^{2,3} AND JAMES A. GRIEVE¹

¹*Quantum Research Center, Technology Innovation Institute, Masdar City, Abu Dhabi, UAE*

²*Centre for Quantum Technologies, 3 Science Drive 2, National University of Singapore, 117543 Singapore*

³*Department of Physics, National University of Singapore, Blk S12, 2 Science Drive 3, 117551 Singapore*

* vadim.rodimin@tii.ae

Abstract: Polarization mode dispersion (PMD) in optical fibers poses a major challenge for maintaining the fidelity of quantum states for quantum communications. In this work, a comprehensive model linking the probability of quantum measurement errors (infidelity) to PMD is developed and validated by experimental measurements of differential group delay and quantum bit error rate (QBER). Our research proposes effective methods to mitigate PMD effects for broadband entangled photons and evaluates the impact of higher-order PMD effects. The model provides an experimentally verified framework for the optimization of commercial quantum key distribution systems in deployed fiber optic lines.

1. Introduction

Quantum communication is a rapidly developing field that focuses on facilitating communication between quantum computers [1–3], and providing secure solutions such as Quantum Key Distribution (QKD) [4]. To connect two quantum computers, a non-local quantum resource called entanglement is required. QKD enables secure communication by exploiting the principles of quantum mechanics, in particular by using non-local entangled polarization states for protocols such as BBM92 [5].

Polarization Mode Dispersion (PMD) occurs in optical fibers, causing wavelength-dependent polarization transformations of light as it travels through the fiber. This phenomenon results from the Differential Group Delay (DGD) between two orthogonal polarization modes of light. In an ideal fiber, light maintains a single polarization state, but real-world fibers always exhibit imperfections and stress, leading to varying propagation speeds for different polarization modes [6]. The polarization state of light in a fiber can be visualized on the Poincaré sphere Fig. 1a. As we change the wavelength of light while maintaining the input polarization, its output polarization state moves on the surface of the Poincaré sphere, illustrating changes in polarization due to PMD. In classical communication, you can use only two orthogonal polarization states and minimize the effects of PMD by aligning them in the direction that has the least distortion. In quantum communications one must use the superposition of orthogonally polarized states [7]. This leads to significant challenges in maintaining the fidelity of quantum states, which is crucial for secure QKD and other quantum communication applications.

In BBM92-type QKD protocols [4,5], we produce bipartite entangled polarization states

$$|\psi\rangle = \frac{|HH\rangle + |VV\rangle}{\sqrt{2}}, \quad (1)$$

defined in terms of the H (horizontal) and V (vertical) basis states. One of the most effective entanglement sources in the optical domain is type-0 Spontaneous Parametric Down-Conversion (SPDC), known for its relatively broad spectrum. Our research employs Periodically Poled Lithium Niobate (PPLN) crystals to generate an SPDC spectrum centered at 1313 nm with an FWHM range of 30-100 nm. Factors such as crystal length, pump bandwidth, focusing

conditions, and temperature influence this spectrum. To obtain polarization-entangled photon pairs, we used the PPLN crystal in a linear displacement interferometer, applying a technique akin to that described in [8].

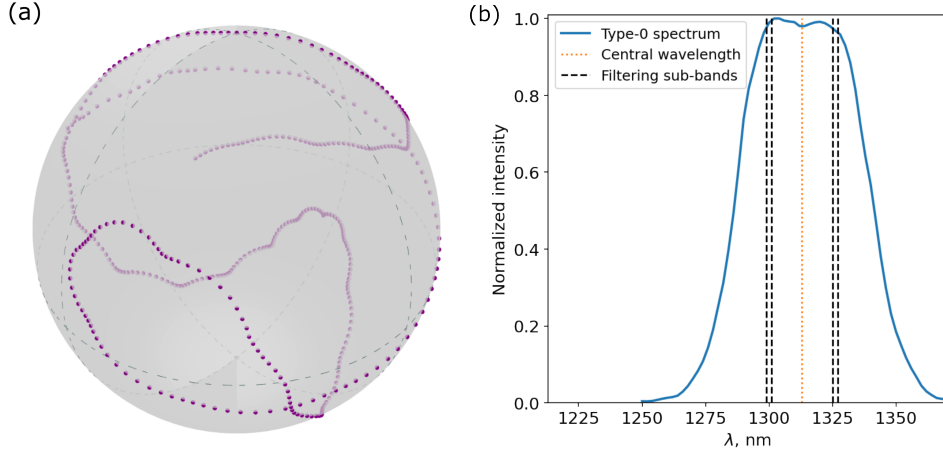


Fig. 1. Necessity of narrow sub-bands filtering due to PMD. (a) Observed polarization trajectory upon propagation through 30 km of typical fiber (ITU-T G.652 specified) [9]. Measured over the range of 1260 - 1360 nm in steps of 0.25 nm; (b) Broadband type-0 SPDC spectrum based on 25 mm of PPLN crystal with the poling period of $12.83 \mu\text{m}$. The pumping wavelength is 656.5 nm.

The photon source creates a superposition state that is uniformly distributed across the Poincaré sphere. At the receivers' locations, the states are measured using either the horizontal/vertical (H-V) or diagonal/anti-diagonal (A-D) bases, or any other four states that form two mutually unbiased measurement bases. These states are aligned on a great circle of the Poincaré sphere, referred to as a 4-state circle. As these states propagate through a fiber, they undergo wavelength-dependent PMD, which fluctuates over time due to environmental changes.

Studies on PMD classify the effect of PMD into first-order PMD and higher-order PMD [10]. First-order PMD considers a constant relative propagation delay between the two Principal States of Polarization (PSPs). In contrast, higher-order PMD involves variations in both the direction of the PSP and the delay value with wavelength. For two orthogonal polarization states, the effect of first-order PMD can be mitigated by aligning the input polarization with the PSPs of the fiber. However, for the previously mentioned 4-state circle, significant first-order PMD effects cannot be eliminated in the same manner. The most practical way to reduce PMD-induced distortions and restore correlations is to narrow the spectral width of the source using narrowband filtering before transmitting the light into the fiber. Fig. 1b shows an example of filtering distant wavelengths, which is convenient for separating entangled photons by channels. However, filtering decreases the brightness of the source, creating a trade-off between the brightness of the transmitted light and the quantum bit error rate (QBER). Our research develops and verifies a model linking channel parameters and the entanglement source bandwidth with the level of distortion experienced in BBM92-type measurements, forming the foundation for future attempts to optimize this trade-off.

The issue of optical dispersion in fibers for QKD applications presents several challenges. Nonlocal dispersion compensation has been proposed [11] and experimentally validated [12, 13] to address chromatic dispersion. With respect to the field of PMD research, studies such as [14–17] provide significant insights. However, from an operational perspective, using these findings directly as an optimization model is challenging. Some PMD compensation works, for

example [18], offer results beneficial for prepare-and-measure protocols but are less applicable to broadband entangled QKD. The model proposed by Muga [19] offers a practical framework aligned with our goals, yet our numerical results differ from theirs.

In the Model Description section, we present a graphical approach linking measurement error probability with PMD. We then provide experimental validation through DGD measurements and QBER analysis in a QKD system. In the Discussion section, we propose methods to mitigate PMD effects for broad-band entangled-based QKD and assess the impact of higher-order PMD effects.

2. Model description

In the literature of PMD studies, the transformation of the polarization state s_{out} in fiber due to the 1st order PMD is described by the PMD vector $\vec{\Omega} = \Delta\tau\vec{p}_1$, where $\Delta\tau$ is the DGD and \vec{p}_1 is the PSP vector [10]. When the light frequency changes from ω_1 to ω_2 , the output polarization state rotates around the PMD vector, as shown in Fig. 2a. The rotation angle is given by the equation

$$\Delta\theta = \Delta\tau(\omega_2 - \omega_1), \quad (2)$$

while second-order PMD considers the variation of the PMD vector's length and orientation with changes in frequency. Consequently, we can describe the actual trajectory of polarization transformation on the Poincaré sphere (Fig. 1a) by evaluating frequency-dependent parameters [20].

Longer trajectories of an output polarization state on the Poincaré sphere corresponds to greater distortions caused by PMD. An important consideration in our context is that the 4-state circle, formed by measurement basis vectors, can be aligned differently with respect to the PMD vector. The maximum total trajectory corresponds to the PMD vector being aligned perpendicularly to the 4-state circle (Fig. 2b). Here, we neglected PMD orders higher than the 1st, which is consistent if we consider small enough trajectory patches. It is possible to decrease PMD distortion by choosing the measurement states such that the PMD vector lies in the 4-state circle. When the states of one basis coincide with PSP vectors, their trajectories shrink to points, so only the states of the other basis contribute to PMD-caused measurement errors (Fig. 2c). A symmetrical case is depicted in Fig. 2d, where the PMD vector also lies in the 4-state circle plane.

Consider a trajectory L on the Poincaré sphere, created by transmitting light with a spectrum evenly distributed within a bandwidth $\Delta\lambda$. When measuring the output light projecting it on a chosen polarization state $|s_0\rangle$, the intensity is directly proportional to the integral of the squared modulus of the projections of the polarization states along the trajectory L onto the selected state $|s_0\rangle$:

$$I \propto \int_L |\langle s(\lambda) | s_0 \rangle|^2 d\lambda \quad (3)$$

Here, the polarization vectors are considered in the Jones space. In the case of single-photon measurements in the basis $\{s_0, s_0\text{_orthogonal}\}$, the measurement error probability p_e can be determined by using the formula

$$p_e = 1 - \frac{1}{\Delta\lambda_L} \int_L |\langle s(\lambda) | s_0 \rangle|^2 d\lambda, \quad (4)$$

below we refer to this as "trajectory integration". One can say that this is the PMD contribution to QBER for a particular state measurement. It is easy to show that p_e is in fact the *infidelity* between the median pure state $\rho_0 = |s_0\rangle\langle s_0|$ and the resulting density matrix

$$\rho(\Delta\lambda) = \frac{1}{\Delta\lambda_L} \int_L |s(\lambda)\rangle\langle s(\lambda)| d\lambda, \quad (5)$$

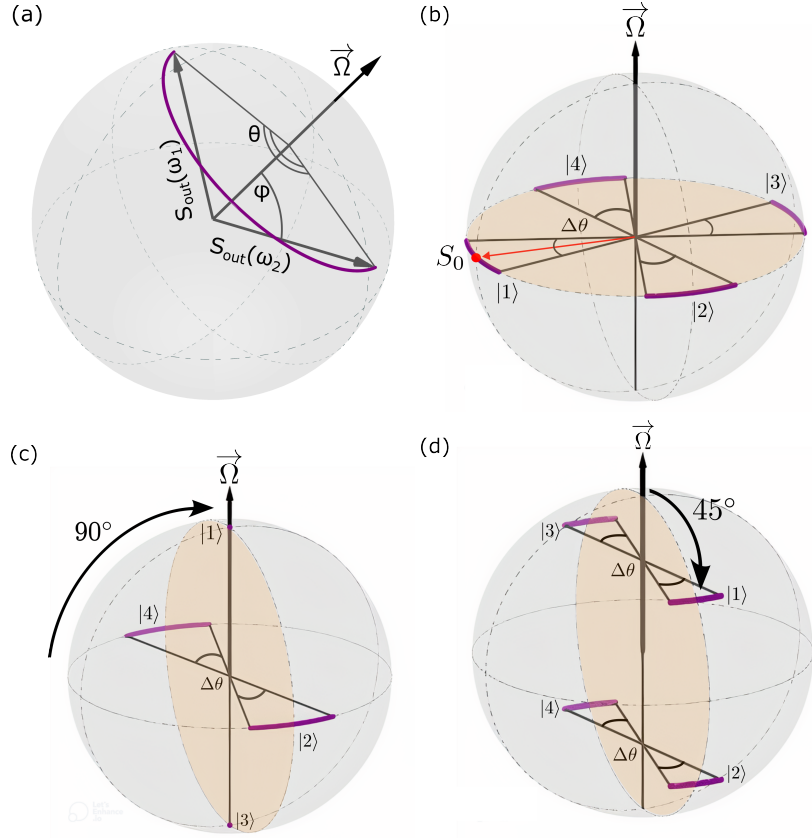


Fig. 2. Polarization trajectories on the Poincaré sphere with wavelength variation. (a) the first-order PMD: output polarization rotates around a PMD vector; (b) special case: PMD vector is orthogonal to 4-state circle plane; (c) special case 1: PMD vector lies in the 4-state circle plane, two states coincide with PSPs; (d) special case 2: PMD vector lies in the 4-state circle plane, all four states distributed symmetrically.

where infidelity is defined as $1 - F(\rho_0, \rho(\Delta\lambda)) = 1 - \left(\text{tr} \sqrt{\rho_0 \rho(\Delta\lambda)} \right)^2$ [21].

When considering a small arc on a great circle formed by an angle $\Delta\theta$ corresponding to the filtering bandwidth $\Delta\lambda$, we tune the measurement basis with a polarization controller that allows us to choose any s_0 for projective measurement. Let s_0 be the central point of the arc Fig. 2b. The resulting infidelity is obtained through integration over all wavelengths

$$p_e = 1 - \frac{2}{\Delta\theta} \int_0^{\Delta\theta/2} \left(1 - \sin^2 \varphi \sin^2 \frac{\theta}{2} \right) d\theta = \frac{\sin^2 \varphi}{2} \left[1 - \text{sinc} \frac{\Delta\theta}{2} \right], \quad (6)$$

where φ is an angle between the polarization state and the PMD vector $\vec{\Omega}$ (Fig. 2a). It has to be mentioned here that the sinc shape of the infidelity is effectively the Fourier transform of the assumed rectangular signal spectrum. Gaussian spectral distribution would result in a Gaussian infidelity shape, and so on.

For the most practically interesting case of relatively small p_e this can be further simplified using Taylor expansion in powers of $\Delta\theta$, to get a useful relation

$$p_e \approx \sin^2 \varphi \frac{(\Delta\theta)^2}{48} \quad (7)$$

From DGD measurements we can find $\Delta\theta$ using eq. (2) that gives us p_e . As a result, we connect the effective infidelity with filtering bandwidth and QKD distance. The relationship between p_e and distance is linear, while p_e and filtering exhibit a quadratic relationship, Fig. 3.

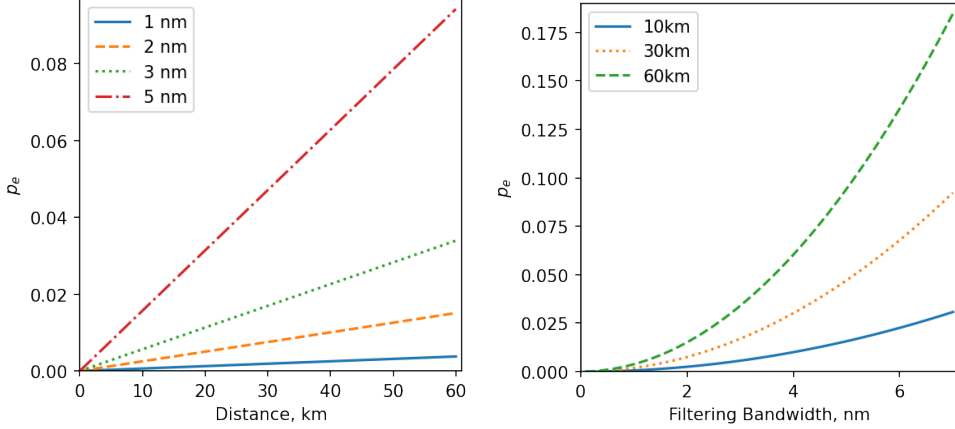


Fig. 3. Statistically average infidelity p_e vs fiber link distance (left) and bandwidth filtering (right). For the calculation, we used PMD link value = $0.05\text{ps}/\sqrt{\text{km}}$

3. Experimental validation

PMD frequency-domain measurements were conducted using a setup similar to [22]. We used a tunable laser Santec TSL-570, manual fiber polarization controller Thorlabs, and polarimeter Thorlabs PAX1000IR2/M. We carried out polarization measurements of various 10 km deployed fiber channels in Masdar City, Abu Dhabi. The Mueller Matrix Method (MMM) [23] was employed for DGD determination from polarization measurements.

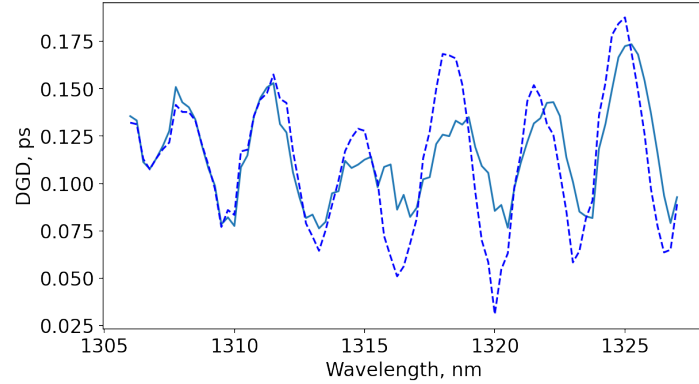


Fig. 4. Differential group delay vs wavelength obtained using MMM [23] method. Two different graphs give an understanding of the reproducibility of the method and correspond to different pairs of input states needed for MMM calculations.

To determine infidelity through numerical integration, we take a polarization trajectory patch on the Poincare sphere, choose a central point s_0 , and integrate along the patch (4). This patch corresponds to the filtering bandwidth $\Delta\lambda$. For a long trajectory, we roll this patch along the trajectory, and this rolling integration provides us with infidelity versus wavelength for a particular

$\Delta\lambda$. However, arbitrary polarization generally does not rotate around the PMD vector along the great circle. A random state can rotate at any $\varphi < \pi/2$ as shown in Fig. 2d or even converge to a point as for states $|1\rangle$ and $|3\rangle$ in Fig. 2c. When we determine infidelity from DGD measurement (7), we assume $\sin\varphi = 1$, corresponding to rotation along the great circle in Fig. 2b. Consequently, DGD infidelity represents an upper limit for the trajectory integration. Therefore, comparing DGD calculation with trajectory integration validates the proposed model, as illustrated in Fig. 5. The slight deviation of the DGD (4) curve from the maximum possible can be accounted for the absence in the model of higher-order PMD effects beyond the first one.

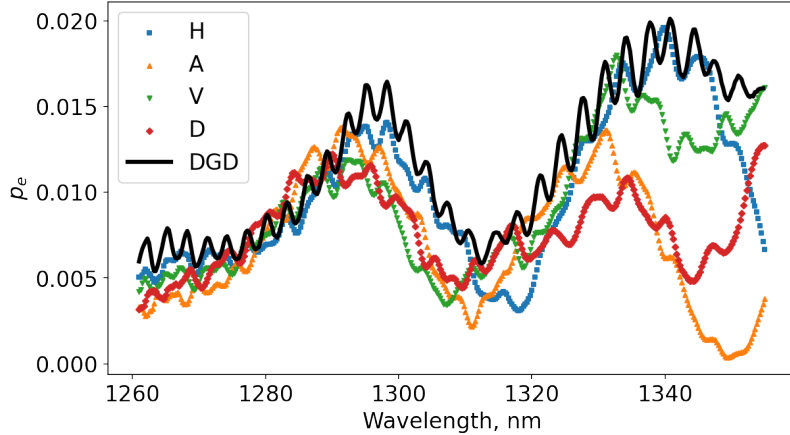


Fig. 5. Infidelity p_e for 5 nm filtering found from DGD measurement (black) using (7) and by trajectories integration (4) for different input polarization states H, V, D, A.

Here, we assess the correspondence of two methods for estimating p_e : numerical trajectory integration (4) and proportionality to DGD squared (7) while altering the filtering bandwidth, Fig. 6. The relationship is quadratic and aligns closely with the proposed model.

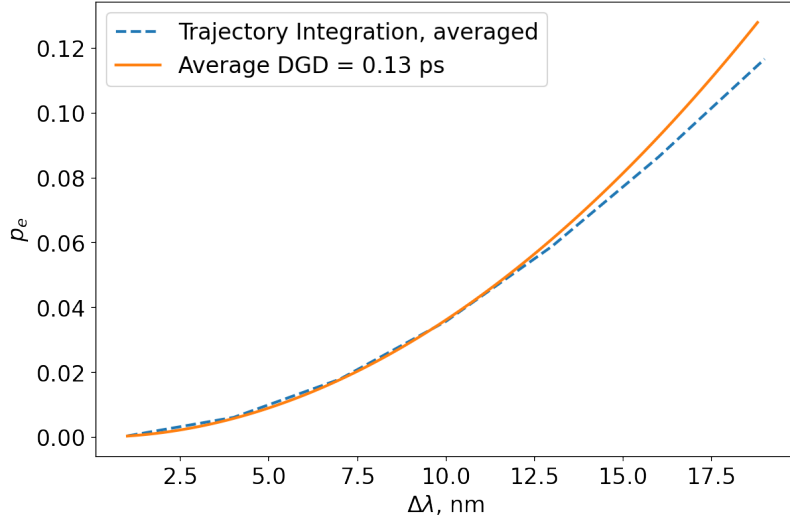


Fig. 6. Comparison of infidelity calculation using DGD approach (7) and trajectory numerical integration (4).

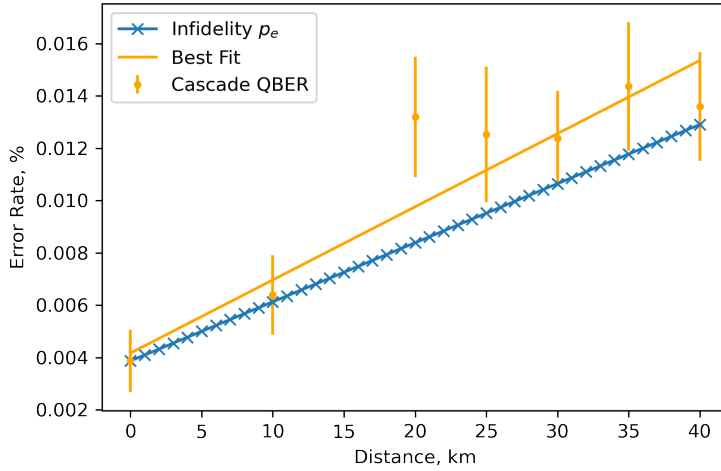


Fig. 7. Measured QBER and modeled infidelity p_e vs. link distance. For the model, we used PMD link value = $0.0474\text{ps}/\sqrt{\text{km}}$ obtained from one of our fibers. Note that the PMD link value can be as high as $0.2\text{ps}/\sqrt{\text{km}}$, based on specifications dictated by international standards [9].

In a real QKD system there are different sources of errors, so it is not straightforward to distinguish PMD-related QBER from the common background. We used a self-made QKD setup designed with a scheme similar to [24], and prepared for real-world deployment. The photon pairs were separated into two channels using fiber Bragg filters with 2nm sub-bands while fiber spools were utilized to make up the distance. Passive basis choice receivers have Rubidium frequency references (AR133-00, Accubeat) to simplify distant synchronization. For on-site detection, we used IDQubes set to 20% detection efficiency. The polarization state in one of the channels was tuned using fiber-squeezing-based polarization controllers (PCD-M02, Luna). We utilized a gradient-descent algorithm to operate the polarization controller to minimize QBER before key exchange. In our experiment, this algorithm was used to lower the estimated QBER until the mean QBER plateaued at a steady state, indicating proximity to a minimum value. Subsequently, key exchange was conducted for 30 minutes to gather sufficient relevant statistics.

The trend of the measured QBER versus link distance (Fig. 7) is very close to the minimum possible due to PMD for a chosen, typical PMD parameter. The overall QBER nearly coincides with PMD-induced errors (infidelity) and demonstrates reasonably linear behavior (R value 0.914). This allows us to conclude that, in our QKD system, the PMD-related QBER dominates.

4. Discussion

The overall impact of the PMD-induced loss of fidelity on the QKD system strongly depends on the orientation of the 4-state circle with respect to the PMD vector $\vec{\Omega}$. For BBM92 protocol (i.e. BB84 bases arrangement) the maximal probability of error occurs when both bases lie on the great circle orthogonal to the PMD vector, Fig. 2b. Each of the four states experience the same maximally possible decoherence (6) at $\varphi = \pi/2$. Detection errors are, thus, equally observed in both bases.

In order to minimize the effect of PMD it is reasonable to align one of the measurement bases with the PMD axis, Fig. 2c. In this case, the first-order PMD-related decoherence disappears for this particular one, while it remains at the maximal level for the other. Formally, it means that the

average PMD-induced QBER is twice as low, as in the worst case. However, from a practical point of view it creates a strong asymmetry between the two bases, which is not always desirable, as it has to be properly accounted during error correction and privacy amplification steps.

A more practical alternative orientation of the bases is when the PMD vector lies in the plane of the 4-state circle, but exactly in the middle of the arc between two adjacent measurement states, Fig. 2d. Due to the factor of $\sin^2 \varphi$ in (6), the effective probability of errors is still twice smaller than in the worst case, but the errors are evenly distributed between the two bases, which could lead to a more balanced operation and, potentially, better overall performance.

Moreover, if the protocol assumes unequal probabilities for the basis choice, as in [25], the resulting error distribution can be fine-tuned to achieve the optimal balance of the error rates with respect to the basis choice asymmetry. In other words, the more probable basis should have a lower QBER by shifting the corresponding states closer to the PMD vector while keeping the latter within the 4-state circle plane.

Interestingly, the average detection error probability for the 6-state protocol [26] with equiprobable bases is completely invariant to the rotations of the bases with respect to the PMD vector. This pinpoints the greater symmetry of the 6-state protocol with respect to the conventional BB84. The distribution of errors between the three bases is, however, dependent on the bases orientation and can be easily symmetrized.

Let us now look at a few practical implementation examples to show available tools of PMD mitigation. For simplicity let us assume that the source generates a singlet state $(|HV\rangle - |VH\rangle)/\sqrt{2}$, which can be obtained from the state (1) by applying Pauli transformation σ_y to either of the qubits. The singlet state, being measured in any basis, always yields perfectly anti-correlated results. Therefore, for establishing QKD it is only required to match two transformations between the source and the two receivers. This can be realized with a single polarization controller, as shown in Fig. 8a. It has to be set to perform the same transformation U , as in the other channel, so $U_1 = U$. However, if there is PMD in one of the channels, it is important to properly orient the measurement bases with respect to the PMD vector. As we show below, this can be done by introducing one more polarization controller.

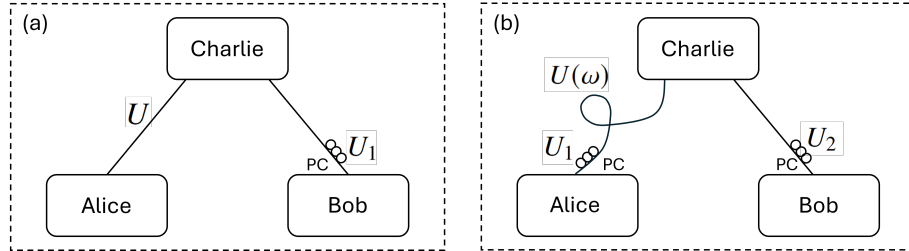


Fig. 8. Configurations with PMD mitigation: (a) local detection; (b) one local one remote measurement. PC – polarization controller, U – unitary transformations of the polarization state.

This configuration is shown in Fig. 8b: one of the photons is detected locally, while the other one passes through the long fiber line with a non-negligible PMD that we denote as a wavelength-dependent unitary polarization transformation $U(\omega)$. For simplicity, we will consider the case when one of the bases is aligned with the PMD vector. This can be done with the use of the Alice's polarization controller placed between the channel and her measurement device. It should be tuned to perform the unitary transformation

$$U_1 = |H\rangle\langle p_1| + |V\rangle\langle p_2|, \quad (8)$$

where $\langle p_{1,2}|$ are the two PSPs.

Now a second polarization controller is required to ensure identical transformations in both channels at some median wavelength ω_0 . It has to be tuned to perform $U_2 = U_1 U(\omega_0)$. In this configuration the PMD does not affect correlations in the $|H\rangle-|V\rangle$ basis and thus, reduces its overall impact. By the choice of (8) it can be further tuned to become symmetric between the two bases or even to shifting most of errors towards the $|H\rangle-|V\rangle$ basis, when it becomes farther from the channel PSPs.

The situation may become even more interesting when two long channels between Charlie and Alice and Bob have their own PMD. Results provided in the present work give a good insight into available tools of PMD mitigation, which could be easily extended to this more complicated case. Also, there is a known phenomenon of non-local PMD compensation proposed in [27] and further elaborated in [28]. It is an interesting task to find practical use cases of this compensation concept in experimental entanglement-based QKD applications. However, it goes beyond the scope of the current manuscript and should be addressed in a separate research initiative.

The above considerations are pertinent when disregarding PMD orders higher than the first one. The higher orders take into account $\vec{\Omega}$ absolute value and direction changes with wavelength. The absolute value change corresponds to a change in the speed of rotation of polarization around $\vec{\Omega}$. In contrast, $\vec{\Omega}$ direction change causes four measurement states to go beyond the plane of the 4-state circle. Let us assess their impact on infidelity.

For $\vec{\Omega}$ absolute value change, let's take the measured dependence of DGD on wavelength (Fig. 4). The DGD exhibits oscillations with a period comparable to 1 nm. This behavior is typical, as similar oscillations are observed in all our measurements and in [29], for example. In two channels (Alice and Bob), we can expect similar oscillations with a random phase. The worst case is when the oscillations are in antiphase in the two channels: the polarization state in one channel advances on the Poincare sphere while it lags behind in the other channel, and vice versa. For saw-like antiphase oscillations, where the oscillation amplitude is half of the average DGD value in each channel, the maximum angle between Alice's and Bob's states $\Delta\theta_{osc} = \Delta\theta_0/4$, where $\Delta\theta_0 = \Delta\lambda_0\langle\Delta\theta\rangle$, and $\Delta\lambda_0$ represents half of the oscillation period for the DGD. In Fig. 4, $\Delta\lambda_0 \approx 0.8$ nm. Consequently, the contribution of DGD oscillations to the measurement error probability $(\Delta\theta_{osc})^2/48$ is an order smaller than the 1st order. In addition, this dispersive effect is constrained by the characteristic quantity of DGD oscillation period $\Delta\lambda_0$.

Fig. 1a provides insight into how $\vec{\Omega}$ rotation contributes to p_e . We consider the rotation contribution to be minimal when the trajectory patch lies in a plane. For the 30 km trajectory, relatively long patches still lie in planes. In other words, for a 2-radian arc, which contributes 8% to p_e , the $\vec{\Omega}$ undergoes minimal rotation.

We can separate $\vec{\Omega}$ rotation along the trajectory and perpendicular one. Considered above DGD oscillations, originate from $\vec{\Omega}$ minor rotations, that resemble orbital nutations in astronomy. So we need to estimate the influence of $\vec{\Omega}$ swing perpendicular to the trajectory. For the 1st order PMD case when two states have no dispersion Fig. 2c, due to $\vec{\Omega}$ rotation, $|1\rangle$ and $|3\rangle$ states no longer lie on the poles but form trajectories. This will be the main (so far unaccounted) contribution into PMD-related infidelity.

Numerical analysis of different trajectory segments of 30 km PMD measurements showed that within a 20 nm bandwidth, the PMD vector draws arcs of about 0.35 rad on the poles. This results in 0.4% of additional infidelity for 2 channels. So we can conclude that higher PMD orders give a certain contribution to infidelity, but it is remarkably smaller than that originated from the 1st one.

5. Conclusion

For QKD optimization, many parameters are used, such as source brightness, channel losses, dark count rate, detection efficiency, and others. These are engaged in optimization models [30, 31] to

maximize key generation rates after the last post-processing stage – privacy amplification. We have expanded these models to take into account PMD-related channel parameters and optimize the filtering bandwidth of broad-band entangled photon sources.

Our model, validated through experimental measurements, shows a quadratic relationship between infidelity and filtering bandwidth, as well as a linear relationship between infidelity and QKD distance. A simple way to mitigate the effects of PMD is to align the measurement bases with respect to the PMD vector in such a way that the PMD vector lies in the 4-state circle plane. This can be achieved using an additional polarization controller in the scheme, minimizing QBER. At the same time, it is possible to achieve a balanced error distribution in the measurement basis.

More detailed experiments, as well as further PMD mitigation exploiting non-local PMD compensation, are left for future work. By understanding and mitigating PMD effects, we can improve the security and reliability of QKD systems. We believe our contributions can potentially benefit QKD, quantum communications, and fiber-optic data transfer.

6. Backmatter

Funding. This project is funded by Abu Dhabi’s Advanced Technology Research Council.

Acknowledgments. We thank Karen Sloyan, Jaideep Singh, Anton Trushechkin, Rodrigo Sebastian Piera and Vlad Revici for support in various aspects of the QKD system and Juan Villegas for support in early stages of our PMD measurements.

Disclosures. The authors declare no conflicts of interest.

Data availability. Data underlying the results presented in this paper are not publicly available at this time but may be obtained from the authors upon reasonable request.

References

1. C. M. Knaut, A. Suleymanzade, Y.-C. Wei, *et al.*, “Entanglement of nanophotonic quantum memory nodes in a telecom network,” *Nature* **629**, 573–578 (2024).
2. E. Togan, Y. Chu, A. S. Trifonov, *et al.*, “Quantum entanglement between an optical photon and a solid-state spin qubit,” *Nature* **466**, 730–734 (2010).
3. K. Nemoto, M. Trupke, S. J. Devitt, *et al.*, “Photonic quantum networks formed from NV- centers,” *Sci. Rep.* **6** (2016).
4. A. K. Ekert, “Quantum cryptography based on bell’s theorem,” *Phys. review letters* **67**, 661 (1991).
5. C. H. Bennett, G. Brassard, and N. D. Mermin, “Quantum cryptography without bell’s theorem,” *Phys. Rev. Lett.* **68**, 557–559 (1992).
6. A. Galartossa and C. R. Menyuk, eds., *Polarization Mode Dispersion* (Springer New York, New York, NY, 2005).
7. C. H. Bennett and G. Brassard, “Quantum cryptography: Public key distribution and coin tossing,” *Theor. Comput. Sci.* **560**, 7–11 (2014). Theoretical Aspects of Quantum Cryptography – celebrating 30 years of BB84.
8. A. Lohrmann, C. Perumangatt, A. Villar, and A. Ling, “Broadband pumped polarization entangled photon-pair source in a linear beam displacement interferometer,” *Appl. Phys. Lett.* **116**, 021101 (2020).
9. T. S. Sector, “G.652 : Characteristics of a single-mode optical fibre and cable,” <https://www.itu.int/rec/T-REC-G.652/en> (2016).
10. L. E. Nelson and R. M. Jopson, “Introduction to polarization mode dispersion in optical systems,” *J. Opt. Fiber Commun. Reports* **1**, 1–33 (2004).
11. J. Franson, “Nonlocal cancellation of dispersion,” *Phys. Rev. A* **45**, 3126 (1992).
12. S. P. Neumann, D. Ribezzo, M. Bohmann, and R. Ursin, “Experimentally optimizing qkd rates via nonlocal dispersion compensation,” *Quantum Sci. Technol.* **6**, 025017 (2021).
13. R. Chua, J. A. Grieve, and A. Ling, “Fine-grained all-fiber nonlocal dispersion compensation in the telecommunications o-band,” *Opt. Express* **30**, 15607–15615 (2022).
14. C. Antonelli, M. Shtaif, and M. Brodsky, “Sudden Death of Entanglement Induced by Polarization Mode Dispersion,” *Phys. Rev. Lett.* **106**, 080404 (2011).
15. M. Brodsky, E. C. George, C. Antonelli, and M. Shtaif, “Loss of polarization entanglement in a fiber-optic system with polarization mode dispersion in one optical path,” *Opt. Lett.* **36**, 43 (2011).
16. H.-T. Lim, K.-H. Hong, and Y.-H. Kim, “Effects of polarization mode dispersion on polarization-entangled photons generated via broadband pumped spontaneous parametric down-conversion,” *Sci. Reports* **6**, 25846 (2016).
17. G. Riccardi, C. Antonelli, D. E. Jones, and M. Brodsky, “Simultaneous decoherence and mode filtering in quantum channels: Theory and experiment,” *Phys. Rev. Appl.* **15**, 014060 (2021).

18. G. B. Xavier, G. Vilela de Faria, G. P. Temporão, and J. P. von der Weid, “Full polarization control for fiber optical quantum communication systems using polarization encoding,” *Opt. Express* (2008).
19. N. J. Muga, M. F. S. Ferreira, and A. N. Pinto, “QBER Estimation in QKD Systems With Polarization Encoding,” *J. Light. Technol.* **29**, 355–361 (2011).
20. M. Shtaif and A. Mecozzi, “Modelling of polarization mode dispersion in optical communications systems,” *J. Opt. Fiber Commun. Reports* **1**, 248–265 (2004).
21. A. J. Baldwin and J. A. Jones, “Efficiently computing the uhlmann fidelity for density matrices,” *Phys. Rev. A* **107**, 012427 (2023).
22. P. Williams, “Pmd measurement techniques and how to avoid the pitfalls,” *J. Opt. Fiber Commun. Reports* **1**, 84–105 (2004).
23. R. Jopson, L. Nelson, and H. Kogelnik, “Measurement of second-order polarization-mode dispersion vectors in optical fibers,” *IEEE Photonics Technol. Lett.* **11**, 1153–1155 (1999).
24. Y. Shi, S. Moe Thar, H. S. Poh, *et al.*, “Stable polarization entanglement based quantum key distribution over a deployed metropolitan fiber,” *Appl. Phys. Lett.* **117**, 124002 (2020).
25. M. Lucamarini, K. A. Patel, J. F. Dynes, *et al.*, “Efficient decoy-state quantum key distribution with quantified security,” *Opt. Express* **21**, 24550–24565 (2013).
26. D. Bruss, “Optimal eavesdropping in quantum cryptography with six states,” *Phys. Rev. Lett.* **81**, 3018–3021 (1998).
27. M. Shtaif, C. Antonelli, and M. Brodsky, “Nonlocal compensation of polarization mode dispersion in the transmission of polarization entangled photons,” *Opt. Express* **19**, 1728–1733 (2011).
28. G. Riccardi, B. T. Kirby, C. Antonelli, and M. Brodsky, “An information-theoretical treatment of nonlocal PMD compensation,” in *Advanced Optical Techniques for Quantum Information, Sensing, and Metrology*, vol. 11295 P. R. Hemmer, A. L. Migdall, and Z. U. Hasan, eds., International Society for Optics and Photonics (SPIE, 2020), p. 112950T.
29. M. Schiano, “PMD measurements on installed fibers and polarization sensitive components,” *J. Opt. Fiber Commun. Reports* **1**, 235–247 (2004).
30. X. Ma, B. Qi, Y. Zhao, and H.-K. Lo, “Practical decoy state for quantum key distribution,” *Phys. Rev. A* **72**, 012326 (2005).
31. A. Tayduganov, V. Rodimin, E. O. Kiktenko, *et al.*, “Optimizing the deployment of quantum key distribution switch-based networks,” *Opt. Express* **29**, 24884–24898 (2021).